Fuel 276 (2020) 118030

Contents lists available at ScienceDirect

Fuel

journal homepage: www.elsevier.com/locate/fuel

Full Length Article

A computational study of burning of vertically oriented leaves with various fuel moisture contents by upward convective heating

Peyman Rahimi Borujerdi, Babak Shotorban*, Shankar Mahalingam

Department of Mechanical and Aerospace Engineering, The University of Alabama in Huntsville, Huntsville, AL 35899, USA

ARTICLE INFO

Keywords:
Pyrolysis
Combustion
Moisture content
Convection
Live fuel

ABSTRACT

Pyrolysis and combustion of a solid fuel representing a vertically oriented leaf of manzanita (Arctostaphylos glandulosa) were computationally investigated. Various fuel moisture content (FMC) values corresponding to four manzanita leaf treatments studied experimentally by others, were considered. The fuel was exposed to an upward stream of hot gases in a computational configuration resembling the experimental setup where leaves were burned. Time evolution of the normalized mass of the leaves was used to validate the simulations against the experimental data. Examining the time history of heat release rate confirmed that increasing FMC delays ignition time. The ignition times in simulations were in good agreement with those determined by empirical correlations for all FMCs. The burnout times were somewhat shorter in simulations than the empirically-determined ones. Simulations showed that thermal, momentum and concentration boundary layers are formed on the leaf faces. The boundary layers played a significant role in heating, and subsequent moisture evaporation and pyrolysis of the leaves. Within the leaves, an evaporation front propagating inward from the edges, was detected. A considerable amount of liquid moisture remained in the leaf after ignition. Accumulation of water and fuel vapor around the leaf, as a consequence of the leaf moisture evaporation and pyrolysis, displaced oxygen, decreasing the oxygen concentration therein. A post ignition time was characterized by a high temperature zone around the leaf. At such times, oxygen consumption by gas phase combustion resulted in a noticeable decrease in oxygen concentration around the leaf. The flaming pattern after ignition was qualitatively in agreement with previously reported experimental observations.

1. Introduction

Burning of elevated foliage, twigs and branches collectively known as the plant crown is an integral part of wildland fires. Specifically, individual leaves play a pivotal role by pyrolysis, ignition and flaming in plant torching and fire spread from one plant to another. This motivated several studies [1–10] to investigate individual dead and live leaves, such as manzanita (Arctostaphylos glandulosa) leaves, under convective and/or radiative heating as the predominant heat transfer mechanisms in fire spread. Manzanita is a common shrub in California chaparral, where fire spread is a topic of interest [11–14].

Pickett et al. [2] burned several individual foliage samples, including horizontally held manzanita leaves, above a flat flame burner (FFB). Exit temperature of hot gases, including ~10 mol% oxygen, from the FFB was measured to be nearly 1,000°C. They found that at the time of ignition, a significant amount of moisture remained in the samples. Moreover, moisture was observed in the leaves at temperatures above 100°C. This observation contradicts the classical model which assumes that all moisture evaporation takes place at 100°C. Shotorban et al. [8] modeled these experiments by modifying Gpyro3D [15] and coupling it with Fire Dynamics Simulator (FDS) [16]. Their computed time evolution of normalized mass and mass loss rate, compared reasonably well with the experimental data [2]. In addition, their model showed that the fuel element acted as a bluff body against the flow exiting the FFB with a stagnation point formed close to the bottom face of the leaf and vortical structures formed behind the opposite face. These flow features played a significant role in the ignition and burning process of the leaf.

Gallacher [7] conducted experiments to investigate the effects of season and heating modes on the burning of foliage from ten live shrubs and conifer fuels. He incorporated a FFB for convective heating and a vertical radiant panel for radiative heating. He positioned the leaves with a vertical orientation above the FFB. His results showed that radiation in itself did not lead to ignition. On the other hand, convection by itself resulted in ignition and when it was combined with radiation, ignition took place earlier. Yashwanth et al. [17] conducted modeling by Gpyro3D coupled with FDS for a setup similar to Gallacher [7], with

* Corresponding author.
E-mail address: babak.shotorban@uah.edu (B. Shotorban).

https://doi.org/10.1016/j.fuel.2020.118030
Received 26 February 2020; Accepted 5 May 2020
Available online 27 May 2020
0016-2361/ © 2020 Elsevier Ltd. All rights reserved.

a radiant panel at 1500 K as the only source of heating. This high temperature was sufficient to initiate ignition at a region in the fuel closest to the radiant panel while regions further away from the panel contained an appreciable amount of moisture. They could not validate their results since experimental data for similar conditions were lacking.

Prince and Fletcher [3] and Prince [4] conducted burning experiments on vertically positioned manzanita leaves subject to convective heating through a set up similar to [7]. They considered four distinct categories of leaves - labeled dry dead (4% dry-mass basis Fuel Moisture Content (FMC)), rehydrated dead (26%), dehydrated live (34%) and fresh live (63%) [3,4]. By investigating the time history of the average normalized mass, they noted that the dead leaves released mass sooner. They also observed that the leaf edges were the first spots to undergo ignition, as they heated more rapidly. It is noted that ignition behavior is dependent on the fuel characteristics. For example, the experiments of McAllister and Finney [18] which studied autoignition of relatively thick woody fuels by means of convective and radiative heating, revealed that at low convective temperatures, the ignition comes from the hot spots in the gas phase, while at high convective temperatures, the ignition occurs near the solid fuel glowing spots.

The present study is in part motivated by the findings of a previous modeling work [8], as to the role of fluid dynamics in pyrolysis, ignition and burning behavior of leaves in upward convective heating. That work was focused on horizontally oriented leaves, as reviewed above, while here the focus is on the vertically oriented ones. The additional intent here is to use modeling to provide more insight into the role of FMC in pyrolysis, ignition and flaming behavior of the leaves subject to convective heating. This paper is organized as follows. First, the models and computational configuration are overviewed in §2. Then, results including the computational data for model validation against experimental measurements, are presented and discussed in §3. Finally, an overall summary and conclusions from this study are given in §4.

2. Computational Model

The modified Gpyro3D [8,15] coupled with FDS [16] was used as the modeling tool in the current study. Gpyro3D solves a set of partial differential equations representing thermochemical and physical processes of a fuel element treated as a porous medium. FDS models the transport of mass, momentum, energy and chemical species in the gas phase surrounding the porous fuel. The details of the Gpyro3D-FDS model used here are discussed in the previous work [8] and references therein. FDS is set to run in the Direct Numerical Simulation (DNS) mode. The effect of soot formation and transport is neglected.

The computational configuration is shown in Fig. 2(a) with a design resembling the experimental setup of [3,4] where burning experiments on manzanita leaves were conducted. Here, the experimental conditions are briefly presented. Manzanita leaves were collected from the branches near Riverside, CA. For the experiments, four leaf treatments were conducted: (1) completely cured (dry mass-basis FMC 4%); (2) rehydrated from a cured condition by the help of a humidity chamber (FMC 26%); (3) dried close to the fiber saturation point (FMC 34%); and (4) slightly dried (FMC 63%). Each leaf was placed in a glass duct that prevented ambient air entrainment. The leaf was held by a cantilever mass balance. To provide convective heating, a FFB was rolled into a position directly under the leaf and the glass cage. The exhaust gases of the FFB were measured ~1000°C and 10 mol% oxygen [4]. The computational setup dimensions are $0.18 \times 0.25 \times 0.32$ m ($x \times y \times z$). Since the flat faces of the leaf are parallel to the FFB upward stream thereby inducing the formation of boundary layers on the leaf faces, a nonuniform mesh in the gas phase domain with a finer resolution near the faces was used. As shown in Fig. 2(b), the central zone of the domain extended from $y = -0.025$ m to $y = 0.025$ m and from $x = -0.09$ m to $x = 0.09$ m was resolved with a computational cell size of $1.50 \times 0.51 \times 1.48$ mm in x, y and z directions, respectively. The rest of the domain has a computational cell size of $1.50 \times 1.51 \times 1.48$ mm.

A thin rectangular solid fuel centered 4 cm above the bottom surface of the domain with dimensions of $23.7 \times 0.51 \times 23.7$ mm represents the leaf. The manzanita leaf has an ellipse like shape [4]. The leaf shape was simplified here because of a computational constraint as both Gpyro3D and FDS are structured grid based models and integrating them to handle the curved shape of the leaf is too complicated, and beyond the scope of the current work. With these dimensions, the surface area is computed 5.62 cm^2 which is identical to the mean measured area reported for manzanita leaves [2]. The initial mass in simulations is set to 0.2165 g for the leaf with FMC of 63%. This value is within the range of measured mass 0.2197 ± 0.0127 g reported for manzanita leaves with FMCs in the range of 44 to 107% [2]. The initial dry mass of the leaves with FMC's other than 63% was set to the initial dry mass of the leaf with FMC of 63% in simulations. A uniform mesh with a grid resolution of $48 \times 6 \times 48$ in x, y and z directions is used for the leaf in the Gpyro3D domain. The leaf is subject to convective heating through hot gases exiting the FFB situated at the bottom surface of the computational domain. The FFB exit opening size is 0.18×0.25 m ($x \times y$). Hot gases with 10 mol% oxygen enter the domain at 1000°C and at a velocity of 0.6 m/s, consistent with the measurement conditions reviewed above [4]. The lateral surfaces of the domain are modeled as solid walls with fixed ambient temperature whereas the top surface is modeled as an open boundary. The initial composition of the dry mass was set to 33 wt% cellulose, 33 wt% hemicellulose and 34 wt % lignin, as obtained by Prince [4] using the data for manzanita leaves from the ultimate analysis of Pickett [19] and correlations proposed by Sheng and Azevedo [20]. To model pyrolysis of the dry fuel, a kinetic scheme with ten reactions proposed by Miller and Bellan [21] for a dry biomass consisting of cellulose, hemicellulose and lignin was utilized. This scheme was previously validated [21,8] against the experimental data of Koufopanos et al. [22]. Moisture evaporation is also described by a first order Arrhenius reaction [23]. The reaction scheme is shown in Fig. 1 with the kinetic parameters given in Table 1. Thermophysical properties of the dry fuel constituents, char and moisture are given in Table 2. Each condensed phase species has its own porosity, which is calculated from the true and apparent density values given in Table 2. The porosity averaged over the condensed phase species at a computational cell is obtained through volumetric averaging [8]. Hence, the average porosity in a computational cell evolves with time, as the composition of the fuel in the cell changes due to moisture loss and charring. The average heat conductivity is similarly calculated while the average specific heat capacity is calculated via mass based averaging [15]. To model the chemical reaction of pyrolysis gases in the FDS domain, a single step reaction of methane with air is used. This simplified approach for modeling combustion of pyrolysis products is reasonable given that the current work is not focused on a detailed flame structure or pollutant emissions from the flame. Here, the combustion is dealt with by an infinitely fast, mixing-controlled combustion model [16].

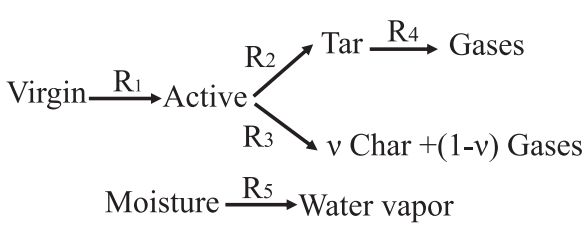

Fig. 1. Generic reaction mechanism for moist fuel [8] involving pyrolysis of dry fuel constituents, viz. cellulose, hemicellulose and lignin [21], and moisture evaporation [30]. Corresponding kinetic parameters are given in Table 1. Here, ν is char formation mass ratio with values 0.35, 0.60, and 0.75 for cellulose, hemicellulose and lignin, respectively [21].

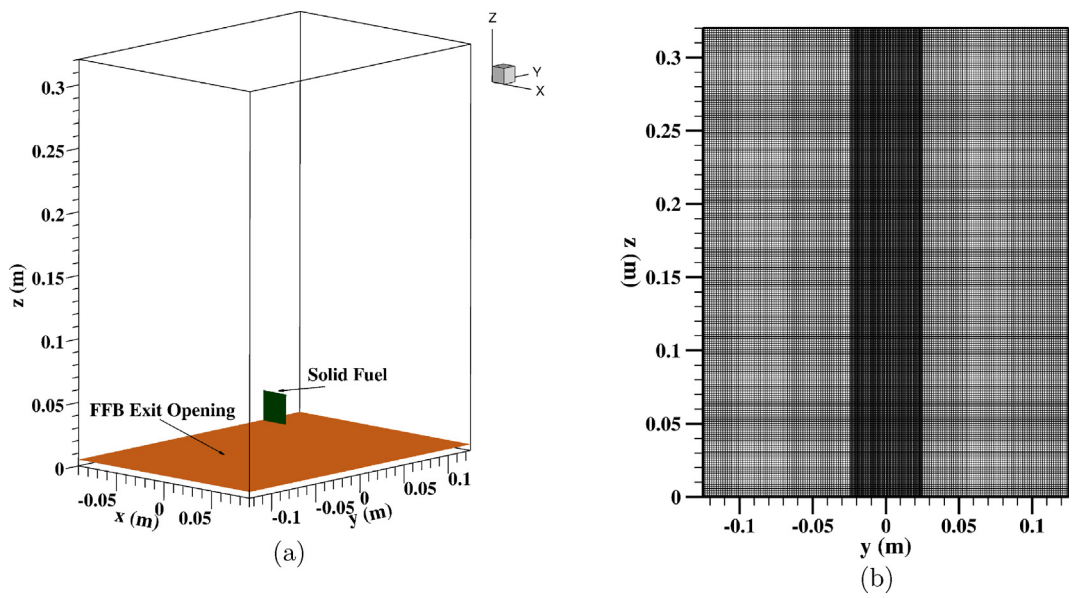

Fig. 2. (a) Isometric view of the computational domain displaying the vertically oriented solid fuel held over an FFB, and (b) A two-dimensional view of the computational mesh on the *yz* plane showing the nonuniformity of the mesh with finer grids in the central zone.

Table 1
Reaction kinetics parameters for moist solid fuel thermal degradation [8] with pyrolysis reactions $R_1 - R_4$ for cellulose (C), hemicellulose (H) and lignin (L) [21], and moisture evaporation R_5 [30].

Reaction	A (1/s)	E (kJ/mol)	Δh (kJ/kg)
R_1 (C)	2.80×10^{19}	242.4	0
R_2 (C)	3.28×10^{14}	196.5	225
R_3 (C)	1.30×10^{10}	150.5	-20
R_1 (H)	2.10×10^{16}	186.7	0
R_2 (H)	8.75×10^{15}	202.4	225
R_3 (H)	2.60×10^{11}	145.7	-20
R_1 (L)	9.60×10^{8}	107.6	0
R_2 (L)	1.50×10^{9}	143.8	225
R_3 (L)	7.70×10^{6}	111.4	-20
R_4	4.28×10^{6}	108	-42
R_5	5.13×10^{10}	88	2260

Table 2
Thermophysical properties of the moist fuel constituents [8]. Here, ρ is apparent density, $\hat{\rho}$ true density, k thermal conductivity, and c specific heat capacity. The species "dry fuel" refers to any of the species cellulose, hemicellulose and lignin, assumed to have identical thermophysical properties [21].

Species	ρ (kg/m^3)	$\hat{\rho}$ (kg/m^3)	k (W/mK)	c (kJ/kgK)	Reference
Moisture	-	1000	0.596	3.9	[23]
Dry fuel	650	2167	0.1256	2.3	[21]
Char	350	2333	0.0837	1.1	[21]

3. Results and Discussion

The time evolution of the normalized mass of the leaf is displayed in Fig. 3, which also includes the experimental data of Prince [4] with 95% confidence intervals. As evident in Fig. 3(a,b), the dead fuels, i.e. leaves with FMC 4% and 26%, release mass faster in both simulations and experiments. However, the model, in comparison to the experimental data, exhibits a delay of one to two seconds in the onset of mass release for the dead fuels. The performance of the model at this initial stage is much better for live fuels as illustrated in panels (c) and (d). For low FMCs, as seen in panels (a) and (b), until the time when the fuel mass is around 50% of its initial mass, the model overestimates the measured mass but after this time it underestimates it. The model performs very well from time zero until ~5.25 s for the leaf with FMC 34%, as seen in panel (c), and until ~8.3 s for the leaf with FMC 63%, as seen in panel (d). After these times, the modeled mass starts deviating from the measured mass with mass lost at a faster rate in simulations. The burnout time defined as the time at which the solid fuel degradation is complete, is larger for all experimental cases.

The discrepancy between the modeled and experimental mass loss could be partly attributed to the solid fuel pyrolysis kinetic model. In fact, Miller and Bellan [21] developed the kinetic model based on the experimental data for specific conditions that do not exactly match the conditions here. For example, a recent analysis of live leaves from several forest plants, excluding manzanita, reveals that while cellulose, hemicellulose and lignin constitute a larger mass fraction of leaf species, they contain appreciable amounts of lipid and protein [24]. It is noted that the pyrolysis kinetic parameters of these two species are not yet known for use in modeling. Furthermore, using a simplified rectangular shape for the leaf may be another contributing factor. Although the overall heating pattern in the leaf to be seen in Fig. 9 is in agreement with the pattern observed in the experiments [3,4], the temperature distribution in the leaf in the experiments could be different due to the effect of leaf edge curvature. Another source of discrepancy could be in representing the combustion of pyrolysis gases with a single-step combustion of methane whereas the chemistry involved in this process is significantly more involved.

Two additional simulations were performed for FMC 63% with grid resolutions different from the one (base resolution) described in §2 in order to evaluate the sensitivity of the results to the grid size. In the first simulation, the Gypro3D cell size was doubled in all three directions without changing the FDS grid size. The difference between the normalized masses calculated in this simulation and the base simulation (Fig. 3d) was less than 0.02 for the entire time. In the second simulation, the cell size in the FDS domain was doubled in the x and z directions without changing the Gpyro3D grid size. The FDS grid size in the y direction, which must be identical to the fuel thickness in the central zone, remained unchanged. The difference between the normalized masses in this simulation and the base simulation was less than 0.05 for the entire time.

Fig. 4(a) shows time history of the mass loss rate (MLR) for different FMCs. Initially, the computed MLR remains zero until about 1 s. During this time interval, the fuel is only heated up without losing mass. The

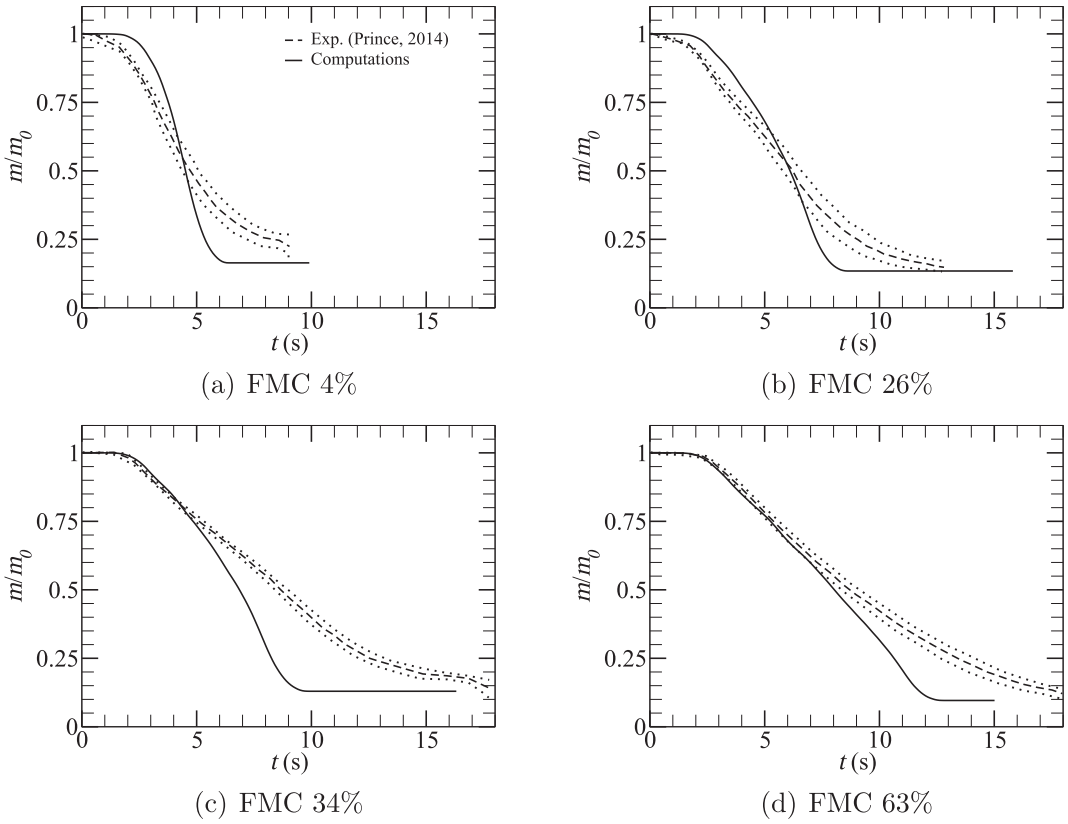

Fig. 3. Time evolution of the leaf normalized mass; dotted lines indicate 95% confidence intervals for experimental data [4].

MLR increases as soon as water evaporation is initiated. After a few seconds, as the leaves attain sufficiently high temperature, pyrolysis commences and contributes to mass loss. Soon thereafter, the MLR exhibits a peak. This occurs due to flame formation around the leaf which provides additional appreciable heating to the leaf, thereby accelerating its degradation. Note that this peak occurs later for larger FMC since additional liquid moisture in the leaf delays both thermal (or Joule) heating and pyrolysis. The MLR starts to decrease and finally becomes zero when the fuel element is completely degraded.

Time history of the heat release rate (HRR) for all four FMC's investigated is shown in Fig. 4(b). Since HRR is predominantly due to gas phase combustion, the time at which HRR first attains a value that is 4% of its peak value is taken as the ignition time. According to Fig. 4(b), ignition time varies from ~2.2 to 3.3 s as FMC changes from 4% to 63%. Ignition time was not reported by Prince [4], Prince and Fletcher [3]. However, in similar experiments by Yashwanth et al. [6] on manzanita leaves with FMC 65%, an ignition time of 3.1 s which is nearly equal to the computed ignition time of 3.3 s for FMC 63%, was reported. It is noted that the dry mass is identical among various FMC cases in the current computational study. Hence, the leaf with a larger FMC, has a larger overall mass, and consequently a larger heat capacity (thermal response time). This effect, combined with the effect of heat of water vaporization causes a leaf with a higher FMC to take longer to heat up and release sufficient fuel vapor for ignition. After ignition, HRR continues to increase up to a maximum for all leaf groups. This time period is longer for a leaf with larger FMC as pyrolysis process is slower. This interval corresponds to the time during which a flame is formed and grows while fuel vapor is released due to solid fuel devolatilization. Note that the peaks of HRR occur almost at the same time as the peaks of MLR since these two quantities are strongly correlated. Subsequently,

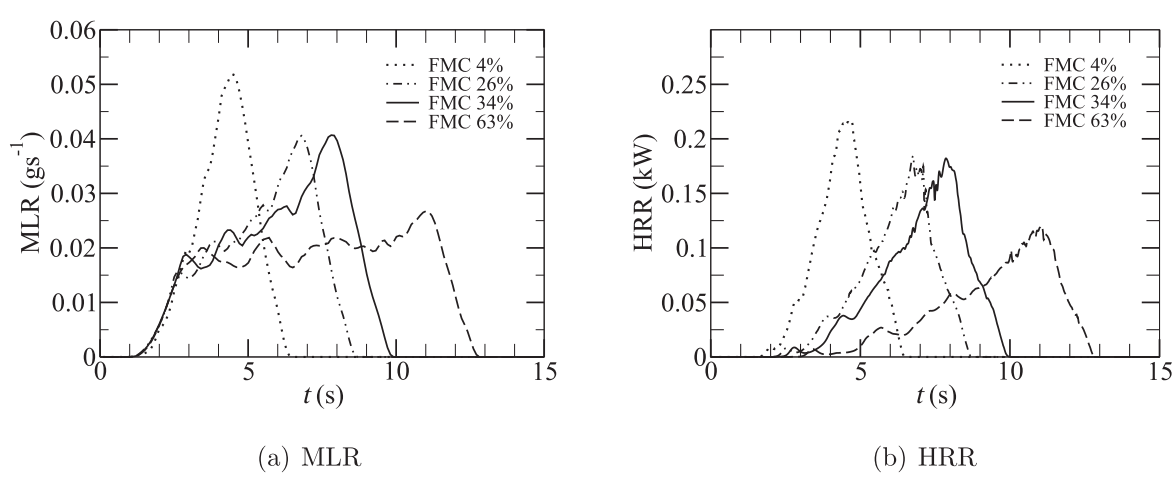

Fig. 4. Time history of (a) the leaf mass loss rate; and (b) the heat release rate in the gas phase.

HRR decreases since the leaf has been mostly converted to char and the pyrolysis process decelerates, consistent with the MLR drop, as evident in Fig. 4(a). The rate of release of fuel vapor into the gas domain decreases and flame extinction commences [25,26]. Finally, HRR becomes zero and a flame ceases to exist. The total heat release by combustion of pyrolysis gases for FMCs 4%, 26%, 34% and 63% were calculated 439, 453, 482, and 444 J, respectively. The relative difference between the minimum and maximum total heat release is about 9%. This relatively small difference is not surprising as the leaves in different cases have an identical dry mass. Since the total heat release is almost the same among all considered FMC cases, the peak of HRR seems to be inversely correlated with the combustion time.

In addition to ignition time, ignition of vegetative fuel in terms of the critical values of other parameters can be discussed [18,27,28]. For example, one may argue that the fuel with higher FMC needs to lose more mass (more moisture) to reach a temperature high enough to cause the release of gaseous fuel needed for ignition. Hence, another associated parameter with ignition is the critical mass loss rate (CMLR), defined as the MLR at ignition. The measurements of McAllister [27], who studied burning of poplar wood samples, revealed that the critical mass flux (which is correlated with CMLR) increased with FMC at a fixed heat flux. In the present work, for leaves with FMCs 4%, 26%, 34%, and 63%, the CMLRs are 0.0062, 0.0138, 0.0178, and 0.0191 g/s, respectively, which exhibit consistency with the previous experiments [27]. Note that as can be seen in Fig. 3, leaves with FMC values of 4%, 26%, 34%, and 63%, have lost about 2%, 5%, 6% and 10% of their initial mass, respectively, at the time of ignition. The experimental data [27] showed a similar trend.

On the other hand, McAllister [27] reported that the critical temperature at ignition was not appreciably sensitive to FMC. Therein, the critical temperature was based on the temperature of a point in the middle of the fuel bed. In the present simulations, the critical temperature changed less than 9% for the FMC values examined. Here, the critical temperature was based on the temperature of the lower corner of the solid fuel where ignition occurred. This ignition location is consistent with the experiments of McAllister and Finney [18] which showed ignition occurred in the vicinity of the solid fuel when the convective stream had relatively high temperature. The reason for this effect is that at relatively high temperatures, the reaction rates are faster and thus the gaseous fuel is released into ambient from the solid fuel at a higher rate. Therefore, near the solid fuel, fuel vapor is generated with a sufficient amount for ignition. In contrast, at relatively low temperatures, reaction rates are slower and pyrolysis products can diffuse further away from the solid fuel and hence ignition takes place in a region that is away from the immediate neighborhood of the fuel [18].

Shown in Fig. 5, are ignition and burnout times versus FMC. The symbols indicate the ignition and burnout times calculated in the present simulations. The curves represent regression based correlations developed by Prince [4] from the experimental data. As could be seen in this figure, the computed ignition times are in agreement with the empirical correlation for the ignition time. On the other hand, it is seen that the model burnout times are overall a few seconds shorter than those given by the burnout empirical correlation. The discrepancy between simulated and empirical burnout times is correlated with the fact that overall, mass is lost at a faster rate in simulations than in experiments, as seen in Fig. 3. Another factor contributing to this discrepancy is the different criteria used in defining burnout times in this modeling effort and in the experimental work [4]. Prince [4] defined the burnout time as the duration between start of the leaf heating and the instance at which the flame height becomes zero. Here, the burnout time was defined as the time at which the leaf ceases to lose mass. It should be noted that the slope of the burnout time versus FMC in the modeling appears to be similar to that in the empirical correlation as seen in Fig. 5.

Contour plots of temperature, oxygen and water vapor mass

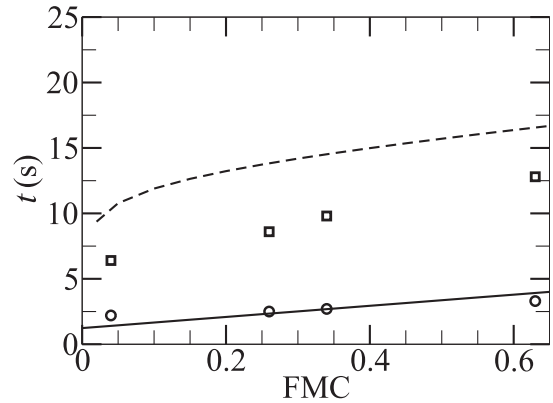

Fig. 5. Ignition and burnout times versus FMC. Circles and squares are ignition and burnout times, respectively, predicted by the present study for four FMCs examined. Solid and dashed lines are ignition and burnout times, respectively, predicted by the empirical correlations in [4].

fractions in the gas domain on a y-z slice with $x = 0$ are shown in Fig. 6 for three time instances. The left, middle and right panels correspond to three time instances before ignition at $t = 2.5$ s, and after ignition at $t = 6$ s and $t = 8.5$ s, respectively. It is noted that at $t = 6$ s, the leaf still contains moisture whereas at $t = 8.5$ s, it is completely dried. The temperature contours in Fig. 6(a) indicate that there is no flame at $t = 2.5$ and the leaf is convectively heated via the thermal boundary layers. These contours are consistent with the contours of oxygen and water vapor mass fractions around and above the leaf, as seen in panels (d) and (g). Specifically, the water vapor and pyrolysis gases released from the leaf displaces the ambient gases away from the fuel. Because of this effect, there is a region where the oxygen mass fraction is smaller, as seen in panel (d). Well after ignition as indicated by the contours of temperature in Fig. 6(b,c), a flame, which can be identified as a region with high temperature, has been formed. From Fig. 6(b,c), it is understood that as time elapses, the flame grows since in this time interval, as can be seen in Fig. 4(a), pyrolysis rate increases, providing more fuel for combustion. The displacement of oxygen away from the solid fuel is also evident in Fig. 6(b,c); otherwise, the flame would be at the leaf surface. In the flame region, oxygen is consumed and its mass fraction is considerably reduced as seen in Fig. 6(e,f). Fig. 6(h,i) show that at $t = 6$s, more water vapor is found near the leaf compared to $t = 8.5$s. The reason is that at $t = 6$s, the leaf still contains moisture and thus in addition to the combustion reaction which generates water vapor, the leaf moisture evaporation also results in accumulation of water vapor around the leaf. On the other hand, at $t = 8.5$s, only combustion reaction contributes to water vapor formation since the moisture evaporation has been completed by this time. Note that flame spread pattern, revealed by temperature contours in Fig. 6(a-c), is consistent with experimental observations [4,3]. Temperature displays asymmetric spatial distribution in Fig. 6(a-c), which is attributed to the inherent flow instabilities near the lateral walls as evident in this figure despite the fact that the boundary conditions themselves are symmetric. These instabilities are also the reason for the lack of complete symmetry in the results of Fig. 7.

Fig. 7 displays the variation of temperature, vertical velocity and water vapor mass fraction in the gas domain in a direction perpendicular to both primary flow direction, i.e., the y axis, and leaf face at $x = 0$m and $z = 0.045$m for two FMCs and three times. Note that the fuel element (not depicted here) extends from -0.255mm to 0.255mm in y. Two thermal boundary layers formed on the faces of the leaf are evident in Fig. 7(a,b), as gas temperature increases with distance from the leaf faces located very close to $y = 0$. At $t = 3$s for FMC 4% in Fig. 7(a), a flame is formed around the leading edge (bottom edge) of the leaf located at $z = 0.02815$m. The flame is the reason for the temperature peaks seen in this figure with values exceeding 1000°C, the

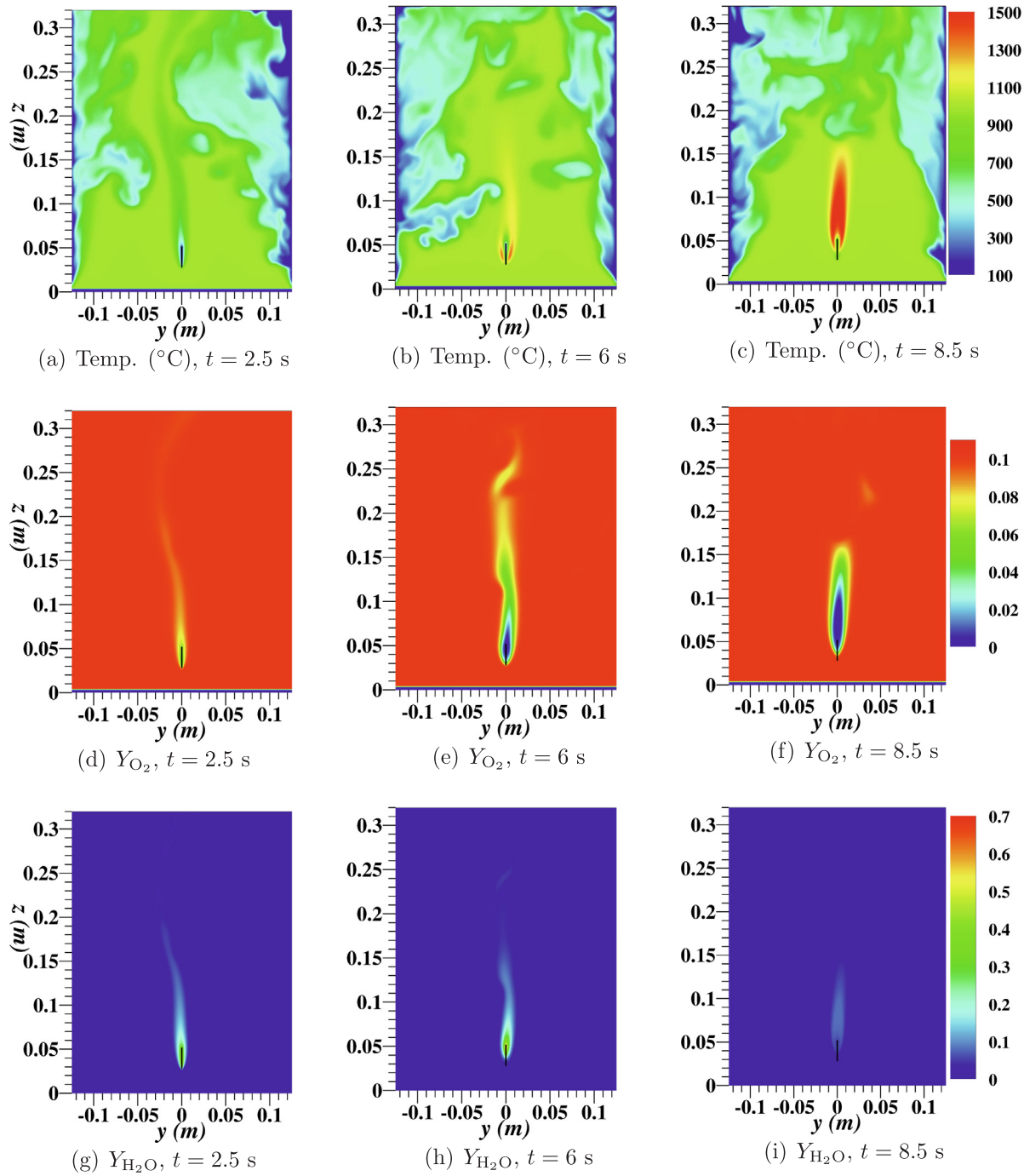

Fig. 6. Contour plots of gas phase temperature, oxygen mass fraction and water vapor mass fraction at t = 2.5, 6, and 8.5s for FMC 34%.

temperature of the free stream exiting the burner. At t = 6s, the gas temperature next to the fuel has risen as the fuel has heated up. Furthermore, at t = 6s fire has propagated upward and there is a reaction zone extending from about $y = -2$mm to $y = -12$mm on the left side of the leaf (and another reaction zone with almost equal span on the right side as well). Consequently, the gas temperature exceeds 1000°C. Outside of the reaction zone, the gas temperature plateaus the free stream temperature. At t = 9s in Fig. 7(a), the fuel has reached the burnout state and since there is no flame, temperature monotonically increases with distance from the leaf face, approaching the free stream temperature. As could be seen in Fig. 7(b), at t = 3s for FMC 34%, temperature increases across the thermal boundary layer and eventually reaches the free stream temperature since at this time no flame has been formed in the gas domain yet. At two later times in this Fig. 7(b), there is a flame and the presence of a reaction zone increases the temperature above the gas temperature at the free stream. It is noted that two momentum boundary layers are also formed on the leaf faces, as evident in Fig. 7(c,d) which show the vertical velocity profile versus y. The vertical velocity vanishes on the leaf face due to the no slip condition and with distance from the fuel surface, it increases across the momentum boundary layer.

Plotted in Fig. 7(e,f) is the mass fraction of the water vapor versus y. The origin of the water vapor around the leaf is mainly the fuel moisture at early times and the combustion reaction at later times. As the fuel heats up, its moisture evaporates and the produced water vapor is transported outside of the fuel. For example, as seen in Fig. 7(e) for t = 3s, there is a significant water vapor mass fraction on the fuel surfaces, which monotonically decreases to zero at the free stream at a

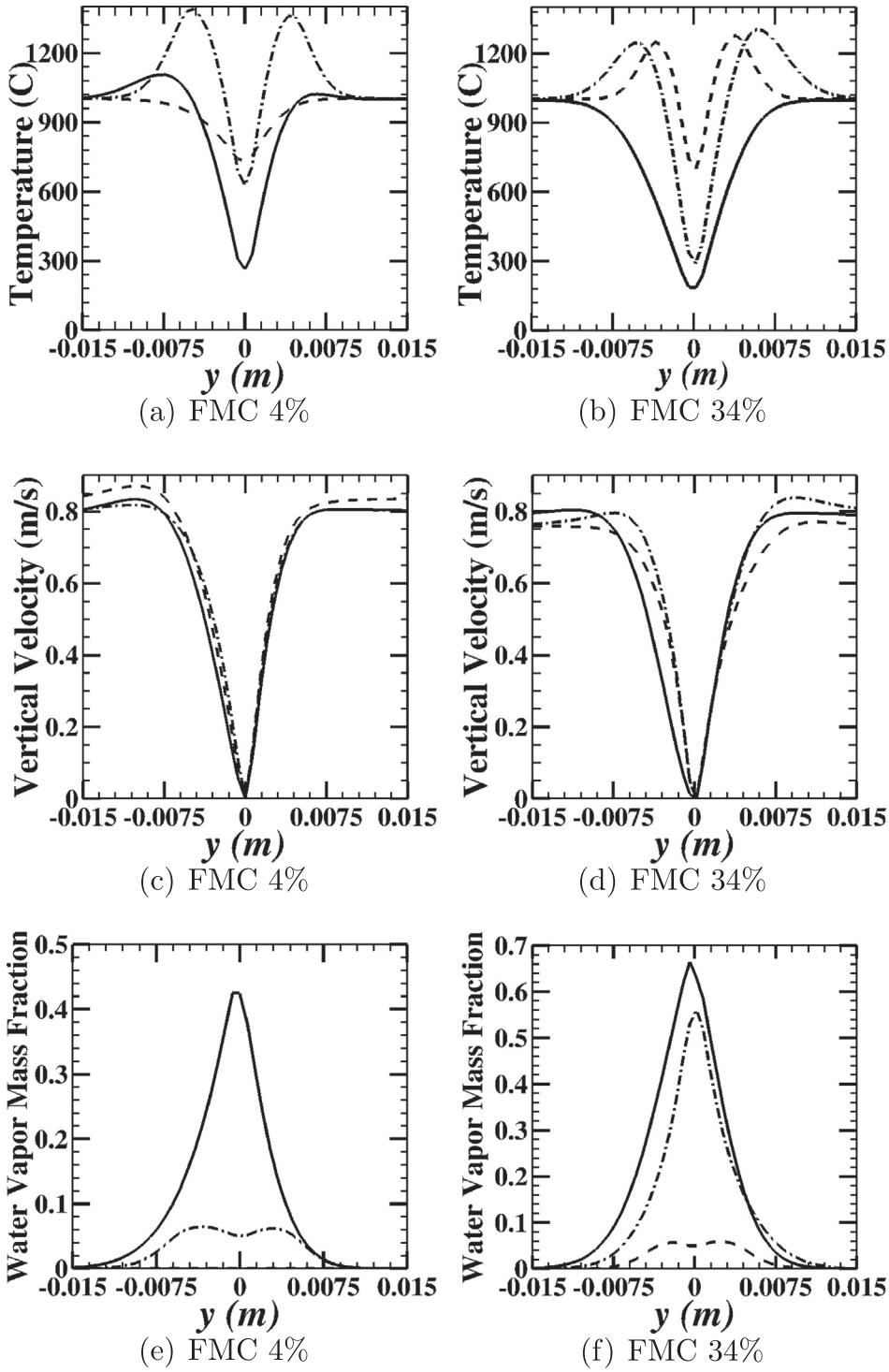

Fig. 7. Variations in (a,b) gas temperature, (c,d) gas vertical velocity, and (e,f) water vapor mass fraction in the gas phase along y direction at t = 3s (solid line), t = 6s (dashed-dotted line), and t = 9s (dashed line) at x = 0m and z = 0.045m. The fuel element (not depicted here) extends from − 0.255mm to 0.255mm in y.

distance which characterizes the concentration boundary layer thickness. In the same panel at t = 6s, it is seen that the water vapor mass fraction around the fuel has substantially dropped. By this time, all moisture of the fuel has evaporated and what is seen here as the mass fraction of the water vapor is produced by the combustion reaction. The y coordinates of the two peaks seen for the water vapor mass fraction in panel (e) at this time are consistent with those of the temperature peaks seen in panel (a) and are associated with the reaction zones. At t = 9s, the mass fraction of the water vapor is zero every where. The reason is that by this time there is no production source for the water vapor since the drying process of the leaf is complete and the flame is gone. For the dehydrated live leaf in panel (f), the water vapor distribution at t = 3s is similar to that for the dry dead leaf in panel (e). However, because of a larger FMC of the dehydrated live leaf, overall, there is a larger amount of water vapor near the leaf for dehydrated live leaf. In panel (f) for t = 6s, water vapor mass fraction decreases slightly, compared to t = 3s. At t = 6s, dehydrated live leaf still contains substantial moisture and thus water vapor continues to be produced by moisture evaporation. It was determined that there is a flame at this time; however, the water vapor is predominantly attributed to the evaporation of moisture from

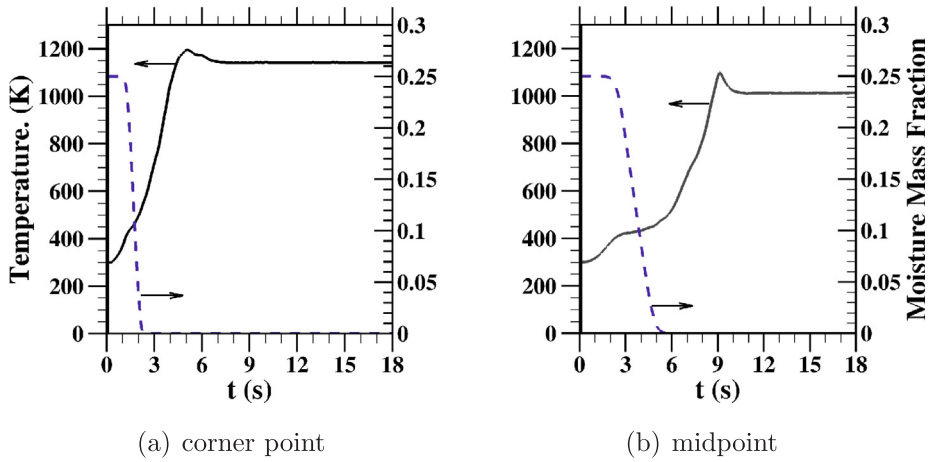

Fig. 8. Time history of temperature and moisture mass fraction for FMC 34% and at two points on the solid fuel left surface: (a) a point located at the lower corner close to the ignition spot with coordinates of $(x, y, z) = (0.01150, -0.000255, 0.02850)$m, and (b) the midpoint with coordinates of $(x, y, z) = (0, -0.000255, 0.04)$m. Note that z-coordinate is measured from the bottom of the computational domain not bottom of the solid fuel.

the fuel. In panel (f) at $t = 9$s, the leaf is dried while undergoing burning and there is a flame. Therefore, at this time, the water vapor is only the product of the combustion reaction.

Fig. 8 displays time evolution of temperature and moisture mass fraction at two distinct points on the left face of the solid fuel with FMC 34%. At a point located at the lower corner with the coordinates $(x, y, z) = (0.01150, -0.000255, 0.02850)$m, the fuel heats up and loses moisture more rapidly because the lower corners receive a higher amount of heat than the rest of the fuel. Consequently, ignition occurs and a flame forms near these corners. The flame provides additional heating to those spots, accelerating the moisture loss and the temperature rise. Temperature reaches a peak at time $t = 5$s, after which it drops slightly since the flame has moved further upward and the heat feedback from the flame to the corner point almost ceases. Eventually, temperature reaches a steady state value of ~ 1150 K (887 °C). At the midpoint of the leaf with the coordinates $(x, y, z) = (0, -0.000255, 0.04)$m, the change of temperature and moisture over time is gradual. After initial heat up, at time $t = 2$s when the temperature is close to the water normal boiling point (373 K), moisture evaporation commences and continues for about 4 s. During evaporation, a temperature plateau is identified as a result of endothermicity of water evaporation. After evaporation completes, temperature rises substantially because of the flame. It is noted that in the experiments [4], the temperature plateaus were observed for FMC 26%, 34% and 63% but not for FMC 4%, and the duration of the plateaus increased with FMC. In the simulations, examining the temperature versus time at the surface midpoint of the leaves with other FMC values revealed similar behavior.

Solid fuel temperature is plotted against x in Fig. 9 for $y = 0$, $t = 6$s and three different z values. Recall that the fuel element has dimension of 0.0237m in both x and z directions. The z values shown in the legend are calculated from the bottom edge (leading edge) of the fuel. Note that $t = 6$s is a post ignition time when there is a flame. The heating pattern identified here is that the solid fuel is heated up from the bottom to the top and from the edges in. A similar pattern was also reported in the corresponding experiments [4]. The leading edge is the closest part of the fuel to the burner. On the other hand, the boundary layers start forming at the leading edge on the fuel faces. As the thermal boundary layer grows in the vertical direction, the convective heat transfer coefficient decreases. Thus, the heat transferred from the hot gases to the solid fuel decreases in the vertical (z) direction. Inside the leaf, the heat from the hotter edges is conducted inward, heating up its interior. The flame can also affect the temperature distribution in the solid fuel. Specifically, it is seen in Fig. 9(a) that near the leaf lateral edges, temperature at $z = 21.85$mm is higher than that at $z = 1.85$mm. The reason is that at the time considered here, there is a flame near the upper part of the leaf, which provides additional heating to this part. Comparing temperature profiles at panels (a) and (b), the leaf with a lower FMC is found to be hotter at the given time. A leaf with a lower FMC has a smaller overall heat capacity, and hence a smaller thermal response time. On the other hand, there is a cooling effect due to the vaporization of leaf moisture. This effect combined with a larger overall heat capacity reduces the rate of heating of the leaf with a higher FMC. Only at $z = 1.85$mm and close to the fuel lateral edges, the leaf with higher FMC is hotter because for this FMC, simulations show a flame formed in the vicinity of the edges at $z = 1.85$mm.

Fig. 10 displays the moisture mass fraction against x for various times at $y = 0$m and $z = 0.01185$m (here, z is measured from the leading edge of the leaf). This location represents a mid-axis of the leaf in x direction. A drying front which propagates inward from the fuel edges is evident in this figure. This drying pattern is consistent with the heating pattern noted in Fig. 9, as the two processes are coupled. The fuel particle attains temperatures high enough to initiate evaporation at its edges first. Thus, moisture loss is first observed near the edges. At later times, when the fuel is heated up by means of heat conduction, the drying front moves inward, and results in moisture evaporation therein. It can be seen in Fig. 10 that moisture still exists in the leaf at $t = 6$s. According to Fig. 9, at the same time and location, temperature is higher than 100 °C, demonstrating that in the leaf, moisture evaporation can occur at temperatures higher than the water normal boiling point. This behavior which was also observed in the previous experiments and computations [2,29] suggests that the classical model of evaporation of all fuel moisture at a constant temperature could not describe the evaporation very accurately. From Fig. 4(b), it is noted that ignition time for leaf with FMC 34% is ~2.8 s. Thus, from Fig. 10, it is understood that the leaf still contains an appreciable amount of moisture after ignition.

4. Conclusions

Pyrolysis, moisture evaporation and burning of a vertically oriented leaf-like fuel under upward convection heating was computationally investigated, using modified Gpyro3D coupled with FDS. The fuel represented a manzantia leaf (Arctostaphylos glandulosa), which was examined under different dry-mass basis FMC conditions of 4%, 26%, 34%, and 63%, consistent with those of dry dead, rehydrated dead, dehydrated live and fresh live manzanita leaves, respectively, previously studied experimentally [3,4]. The computational configuration resembled the setup used in the experiments. For dead leaves, until the time when the fuel mass was nearly 50% of its initial mass, the model

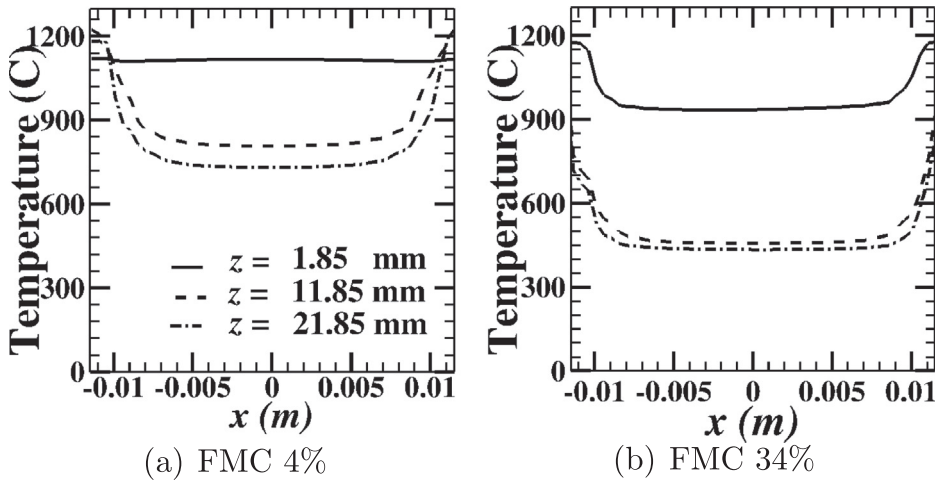

Fig. 9. Variations in the solid fuel temperature with x on $y = 0$ slice at $t = 6$s. The slice passes through the fuel element centroid and $t = 6$s is a post-ignition time.

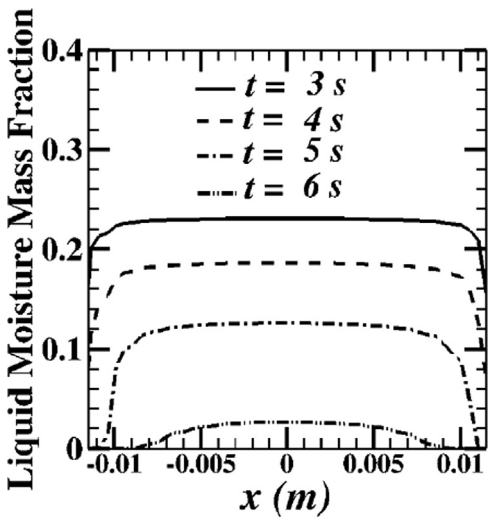

Fig. 10. Liquid moisture mass fraction against x in the solid fuel at $z = 0.01185$m, $y = 0$m, and at different times for FMC 34%.

overpredicted the experimentally measured mass but after this time, the model underpredicted it. As to how the leaf mass evolved in time, the model exhibited a very good match with the experiments until ~5.25 s for the dehydrated live leaf, and until ~8.3 s for the fresh live leaf. After these times, the modeled mass was lost more rapdily than the measured mass. In simulations, time history of the mass loss rate exhibited a peak value corresponding to the peak of HRR. With the increase of FMC, the peak decreased while the peak time increased. However, the total heat release by combustion was not very sensitive to FMC since the dry masses of the fuels with different FMC values were identical. Investigation of the time history of HRR confirmed that the ignition time increased with FMC. The critical mass loss rate defined as the mass loss rate at ignition time increased with FMC while the critical temperature was not appreciably affected by FMC. Since the leaf faces were parallel to the convective streams, boundary layers were formed on the leaf faces. The resulting thermal, momentum and concentration boundary layers played a critical role in heating, and subsequently moisture evaporation and pyrolysis. Examining the heated fuel revealed an evaporation front which propagated from the edges towards the interior. The fuels with 34% and 63% FMCs contained considerable moisture at the ignition time. This effect was also observed in the previous experiments. Before ignition, the water vapor produced by moisture evaporation in the leaf was released into the gas domain and a region with a high mass fraction of water vapor was formed near the fuel. The released water vapor and fuel vapor displaced the oxygen and reduced its mass fraction near the fuel. Since the leaf with FMC 34% had higher moisture content compared to the one with FMC 4%, more water vapor and more oxygen displacement were observed in the region near the leaf before ignition. After ignition, a high temperature reaction zone around the leaf was identified. Due to the combustion reaction, the oxygen mass fraction decreased noticeably while water vapor accumulation was observed. The flame spread and propagation pattern determined by examining the temperature contours at several time instants after ignition was found in agreement with the observations in the previous experiments.

CRediT authorship contribution statement

Peyman Rahimi Borujerdi: Methodology, Software, Validation, Formal analysis, Investigation, Data curation, Writing - original draft, Visualization. **Babak Shotorban:** Formal analysis, Methodology, Software, Validation, Investigation, Writing - review & editing, Supervision, Project administration, Funding acquisition. **Shankar Mahalingam:** Formal analysis, Investigation, Writing - review & editing, Funding acquisition.

Acknowledgments

The authors acknowledge the useful discussions with T. H. Fletcher of BYU, D. R. Weise of USDAFS, and M. A. Dietenberger of USDAFS. This work was supported by DOD/EPA/DOE Strategic Environmental Research and Development Program project RC-2640 administered by the USDA Forest Service PSW Research Station through cooperative agreement JV-11272167-025 with UAH. High performance computing resources and technical support provided by the Alabama Supercomputer Authority are appreciated.

References

[1] Engstrom J, Butler J, Smith S, Baxter L, Fletcher T, Weise D. Ignition behavior of live california chaparral leaves. Combustion Science and Technology 2004;176:1577–91.
[2] Pickett BM, Isackson C, Wunder R, Fletcher TH, Butler BW, Weise DR. Experimental measurements during combustion of moist individual foliage samples. International Journal of Wildland Fire 2010;19:153–62.
[3] Prince DR, Fletcher TH. Differences in burning behavior of live and dead leaves, Part 1: Measurements. Combustion Science and Technology 2014;186:1844–57.
[4] Prince DR. Measurement and modeling of fire behavior in leaves and sparse shrubs PhD dissertation Provo, UT: Brigham Young University; 2014.
[5] J.R. Gallacher, V. Lansinger, S. Hansen, D. Jack, D.R. Weise, T.H. Fletcher, Effects of season and heating mode on ignition and burning behavior of three species of live fuel measured in a flat-flame burner system, in: Spring Technical Meeting of the Western States Section of the Combustion Institute, Pasadena, CA, 2014.

[6] Yashwanth BL, Gallacher J, Shotorban B, Mahalingam S, Fletcher TH, Weise DR. Experimental and numerical investigation of the effect of heating modes and moisture content on pyrolysis and ignition of live fuels. in: 9th US National Meeting Organized by the Central States Section of the Combustion Institute. Cincinnati, OH; 2015.
[7] J.R. Gallacher, The influence of season, heating mode and slope angle on wildland fire behavior, PhD dissertation, Brigham Young University, Provo, UT, 2016.
[8] Shotorban B, Yashwanth BL, Mahalingam S, Haring DJ. An investigation of pyrolysis and ignition of moist leaf-like fuel subject to convective heating. Combustion and Flame 2018;190:25–35.
[9] Safdari M-S, Amini E, Weise DR, Fletcher TH. Heating rate and temperature effects on pyrolysis products from live wildland fuels. Fuel 2019;242:295–304.
[10] Amini E, Safdari M-S, Weise DR, Fletcher TH. Pyrolysis kinetics of live and dead wildland vegetation from the southern united states. Journal of Analytical and Applied Pyrolysis 2019;142:104613.
[11] Weise DR, Zhou X, Sun L, Mahalingam S. Fire spread in chaparral–'go or no-go?'. International Journal of Wildland Fire 2005;14:99–106.
[12] Weise DR, Koo E, Zhou X, Mahalingam S, Morandini F, Balbi J-H. Fire spread in chaparral–a comparison of laboratory data and model predictions in burning live fuels. International Journal of Wildland Fire 2016;25:980–94.
[13] Li J, Mahalingam S, Weise DR. Experimental investigation of fire propagation in single live shrubs. International journal of wildland fire 2017;26:58–70.
[14] Prince D, Shen C, Fletcher T. Semi-empirical model for fire spread in shrubs with spatially-defined fuel elements and flames. Fire Technology 2017;53:1439–69.
[15] Lautenberger C. Gpyro–A Generalized Pyrolysis Model for Combustible Solids, Technical Reference Version 0.8, Reax Engineering. Berkeley, CA: Inc.; 2014.
[16] McGrattan K, Hostikka S, McDermott R, Floyd J, Weinschenk C, Overholt K. Fire dynamics simulator technical reference guide Volume 1: Mathematical Model, Special Publication 1018–6, U.S. Department of Commerce. National Institute of Standards and Technology 2013.
[17] Yashwanth BL, Shotorban B, Mahalingam S, Lautenberger CW, Weise DR. A numerical investigation of the influence of radiation and moisture content on pyrolysis and ignition of a leaf-like fuel element. Combustion and Flame 2015;86:1781–8.
[18] McAllister S, Finney M. Autoignition of wood under combined convective and radiative heating. Proceedings of the Combustion Institute 2017;36:3073–80.
[19] B.M. Pickett, Effects of moisture on combustion of live wildland forest fuels, PhD dissertation, Brigham Young University, Provo, UT, 2008.
[20] Sheng C, Azevedo J. Modeling biomass devolatilization using the chemical percolation devolatilization model for the main components. Proceedings of the Combustion Institute 2002;29:407–14.
[21] Miller RS, Bellan J. A generalized biomass pyrolysis model based on superimposed cellulose, hemicelluloseand lignin kinetics. Combust. Sci. Technol. 1997;126:97–137.
[22] Koufopanos C, Lucchesi A, Maschio G. Kinetic modelling of the pyrolysis of biomass and biomass components. The Canadian Journal of Chemical Engineering 1989;67:75–84.
[23] Bryden KM, Ragland KW, Rutland CJ. Modeling thermally thick pyrolysis of wood. Biomass and Bioenergy 2002;22:41–53.
[24] Matt FJ, Dietenberger MA, Weise DR. Summative and ultimate analysis of live leaves from southern us forest plants for use in fire modeling. Energy & Fuels 2020;34:4703–20. https://doi.org/10.1021/acs.energyfuels.9b04107.
[25] Tihay V, Simeoni A, Santoni P-A, Bertin V, Bonneau L, Garo J-P, Vantelon J-P. On the interest of studying degradation gases for forest fuel combustion modeling. Combustion Science and Technology 2008;180:1637–58.
[26] Tihay V, Santoni P-A, Simeoni A, Garo J-P, Vantelon J-P. Skeletal and global mechanisms for the combustion of gases released by crushed forest fuels. Combustion and Flame 2009;156:1565–75.
[27] McAllister S. Critical mass flux for flaming ignition of wet wood. Fire Safety Journal 2013;61:200–6.
[28] Lin S, Sun P, Huang X. Can peat soil support a flaming wildfire? International Journal of Wildland Fire 2019;28:601–13.
[29] Rahimi Borujerdi P, Shotorban B, Mahalingam S, Weise DR. Modeling of water evaporation from a shrinking moist biomass slab subject to heating: Arrhenius approach versus equilibrium approach. International Journal of Heat and Mass Transfer 2019;145:118672https://doi.org/10.1016/j.ijheatmasstransfer.2019.118672.
[30] Bryden KM, Hagge MJ. Modeling the combined impact of moisture and char shrinkage on the pyrolysis of a biomass particle. Fuel 2003;82:1633–44.